

Corrosion Rate-Based Adjustment of Plastic Hinge Parameters of Corroded RC Elements

Mustapha BENREDOUANE¹

Nouredine BOURAHLA^{2*}

Anouar GHODBANE³

Hala KHALFAOUI⁴



ABSTRACT

In line with the trend towards predictive seismic codes adopting the performance-based design method, this paper presents an integrated protocol to determine the degraded hysteresis parameters of corroded RC hinges based on relationships developed for this purpose together with a calibration procedure using the random-mutation hill-climbing algorithm. The adjustment procedure is integrated into the material library of the OpenSees software and used to perform nonlinear dynamic analyses to investigate the seismic performance of a typical bridge with affected piers at different corrosion levels. In practice the proposed procedure permits to assess the seismic performance of existing or new structures for a given corrosion rate distribution.

Keywords: Hysteresis degradation parameters, reinforcement corrosion, nonlinear dynamic analysis, corroded RC bridge pier.

1. INTRODUCTION

Corrosion of steel reinforcement, alkali-silica reaction, freeze-thaw damage, and sulfate attack are some of the age-related degradation mechanisms for RC structures. Among these mechanisms, the corrosion of steel has been identified as the most widespread and predominant mechanism responsible for the deterioration of RC structures [1,2]. Extensive

Note:

- This paper was received on December 6, 2022 and accepted for publication by the Editorial Board on October 20, 2023.
- Discussions on this paper will be accepted by May 31, 2024.
- <https://doi.org/10.18400/tjce.1214088>

1 National School of Public Works, LTPITE Laboratory, Algiers, Algeria
m.benredouane@enstp.edu.dz - <https://orcid.org/0000-0003-3680-8258>

2 National Polytechnic School, Civil Engineering Department, Algiers, Algeria
Nouredine.bourahla@g.enp.edu.dz - <https://orcid.org/0000-0002-1377-5943>

3 National Polytechnic School, Civil Engineering Department, Algiers, Algeria
anouar.ghodbane@g.enp.edu.dz - <https://orcid.org/0009-0008-8832-2544>

4 National Polytechnic School, Civil Engineering Department, Algiers, Algeria
hala.khalfaoui@g.enp.edu.dz - <https://orcid.org/0009-0003-1364-6636>

* Corresponding author

research work has contributed to elucidate many aspects related to the corrosion of steel reinforcement. At a fundamental level, the initiation and propagation of corrosion in steel reinforcement, which has been addressed in many research programs documented in the literature [3,4] constitutes an essential issue for the service life assessment of RC structures subjected to corrosion [5,6].

Of particular interest is the effect of corrosion on the performance of structures in seismic-prone zones [7-11]. Akiyama and Frangopol [12] proposed a framework to integrate the corrosion effect in terms of airborne chloride hazard probability in the assessment of the seismic performance of bridge piers. Similarly, Choe et al. [13] evaluated seismic fragility curves based on a probabilistic model of chloride-induced corrosion. Following the trend in the generalization of seismic fragility analysis as a corrosion time-dependent concept, Hu et al. [14] proposed a framework and applied it to determine the seismic damage of an aging four-span continuous RC bridge. Using a different approach, Domaneschi et al. [15] investigated the coupling of corrosion and earthquake action on bridge piers to predict the early collapse under such conditions.

It is clear that these frameworks help predict life service and potential damage to structures under seismic threats. Nonetheless, there is a pressing need for the precise assessment of existing deteriorated structures for rehabilitation or other purposes. To fulfil this demand, several experimental studies [16-18] and numerical techniques have been developed to provide practical assessment modeling tools [19,20].

Owing to the complexity and variability of the corrosion phenomena affecting the steel reinforcement of structural elements subjected to seismic loading, it is essential to provide transparent and explicit practical methods that express the relationships between a factor characterizing the corrosion level of a structural element that can be measured in situ or predicted by a time-dependent approach and the numerical model parameters that control the structural deterioration.

In this study, the modified peak-oriented model proposed by Ibarra-Medina-Krawinkler (MODIMK) [21] was chosen as a reference hysteresis model and corrected to account for changes in the properties and deterioration parameters using relationships developed for this purpose. These relationships link the mechanical properties and degradation parameters of the hysteresis loop to the corrosion-level factor. They were integrated into the existing hysteresis model within the material library of the OpenSees software [22].

The proposed model was calibrated using available experimental data for five RC columns with different levels of reinforcement corrosion. Taking advantage of the explicit model, nonlinear dynamic analysis was performed to investigate the performance of a typical RC bridge with piers having different levels of corrosion.

2. MODELING APPROACH OF A CORRODED PLASTIC HINGE

The approach used in this paper is based on the integration of the effect of aging due to the corrosion of reinforcement into a hysteresis model of a plastic hinge of a RC element. The modified Ibarra-Medina-Krawinkler (MODIMK) Peak-Oriented model takes into account six different mechanisms of deterioration: Basic strength deterioration, post-yielding, post-capping, unloading stiffness, reloading stiffness, and pinching. The model is ideal for the

management of degradation phenomena, henceforth, it is adopted to incorporate the deteriorating effect of the corrosion of the reinforcement.

The MODIMK model requires the specification of 23 parameters, where seven parameters at least are calibrated using experimental data.

Further to the initial calibration of the model parameters [21], subsequent studies have been carried out in order to provide explicit and simplified equations to predict the model parameters. Haselton et al. [23] proposed a calibration procedure based on 255 RC column tests and developed a set of equations that can be used to calculate the parameters necessary for the development of the complete "backbone" curve and establish a hysteresis degradation rate knowing only some of the physical and geometric characteristics of a reinforced concrete section. The equations of the parameters which potentially can be affected by the steel reinforcement corrosion are used in this study to calculate the initial rigidity K_e , the plastic rotations capacity (θ_p), the post capping rotation capacity (θ_{pc}) and the post-yield hardening stiffness characterized by the ratio of the maximum moment capacity and the yield moment capacity (M_c/M_y).

The yield moments (M_{y+} and M_{y-}) are estimated using the formulae given by Panagiotakos et al. [24]. However, the cyclic degradation parameters ($\lambda_A, \lambda_K, \lambda_S, \lambda_C$) and their exponents (C_A, C_K, C_S, C_C), will be estimated by a calibration procedure using experimental hysteresis loops available in the literature.

3. HYSTERESIS LOOP PARAMETERS FOR A CORROSION LEVEL (CL)

The degradation of RC structures by corrosion is a very complex phenomenon and involves multiple effects. The visual aspects of the degradations are mainly corrosion-spots, cracks in the vicinity of the rebars, spalling and even the splitting of the concrete cover. The effect on the structural capacity of a RC element, particularly on the dynamic potential expressed in terms of the hysteresis loop parameters, is illustrated in Fig 1.

As mentioned before, the 'MODIMK' model is controlled by several parameters associated with the geometric and mechanical properties of the RC element. Thus, in the first instance, a corrosion level (CL) is defined to characterize the deteriorated RC element and used to determine the altered geometric and mechanical characteristics of the model.

These functions are implemented in the OpenSees and used to simulate series of experimental tests of columns degraded by accelerated (artificial) corrosion at increasing levels. A calibration process is performed to match the numerical and experimental hysteresis loops in order to determine the best fit of the deterioration parameters (λ_i and c_i) for different corrosion rates Fig. 2.

3.1. Characterization of the Corrosion in Existing Elements and Structures

Precise assessment of existing structures subjected to corrosion depends on the accuracy of the evaluation of the degree and locations of the corrosion on the structural elements which are needed to fine-tune the hysteresis parameters at potential plastic hinges. Although, measuring the corrosion rate is difficult, numerous methods exist in the literature for researchers and engineers to evaluate and appreciate the degree of corrosion of existing structures.

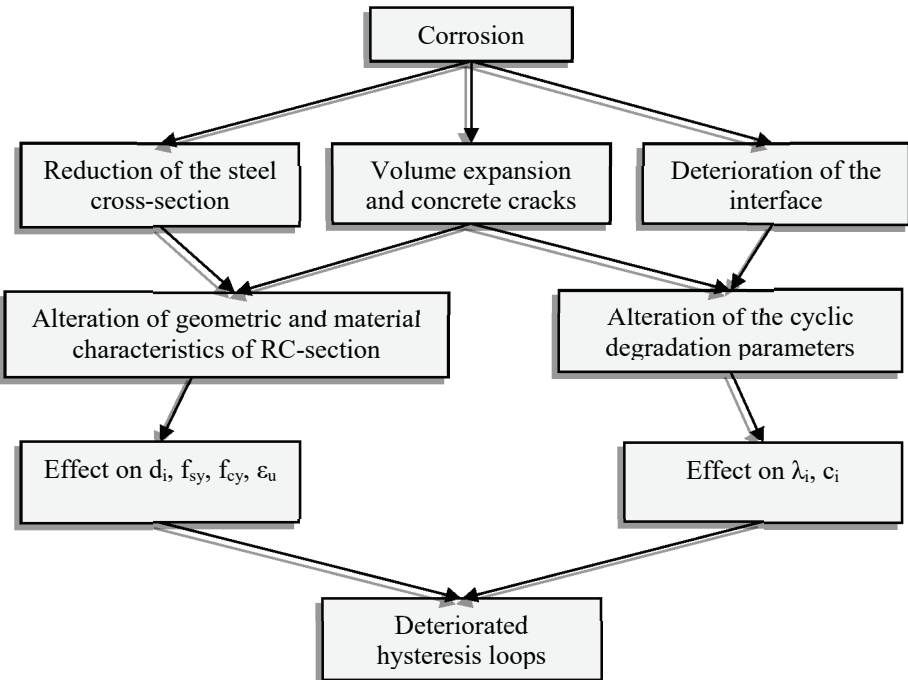


Figure 1 - Effect of the corrosion of reinforcement on the hysteresis loop

In this research work, the corrosion level, CL , is the factor used to characterize structural damage related to aging. It is defined as the average mass loss of rebar.

$$CL = \frac{\Delta w}{w} \times 100 \% \quad (1)$$

- Δw is the mean mass loss of corroded rebars.
- w is the mass of the original rebars.

If the corrosion is homogeneous, over an average surface of the rebar, the level of corrosion can be expressed in terms of corroded and uncorroded cross sections A_c and A_i respectively or in terms of corroded and uncorroded diameters d_c and d_i as follows:

$$CL = \frac{(A_i - A_c)}{A_i} \times 100 \quad (2)$$

$$CL = \left[1 - \frac{A_c}{A_i} \right] \times 100 \quad (3)$$

$$CL = \left[1 - \left(\frac{d_c}{d_i} \right)^2 \right] \times 100 \quad (4)$$

In practice, the corrosion level can be obtained by measurement of the residual diameter d_c or by means of techniques that correlate the width of external cracks with the reduction of the cross-section of the reinforcement bar [25-28].

Other techniques based upon direct measurement of the corrosion current density (i_{corr}), using the linear polarization resistance LPR method or indirect predictions method using non-destructive resistivity measurements [29], are suitable to predict the corrosion current density in a specific location of a structural element at a period of time during its life service.

The conversion of the current density i_{corr} to a corrosion level CL can be obtained using one of the formulae available in the literature such as the expression proposed by Du et al. [30]:

$$CL = 0.046 \frac{i_{corr}}{d_i} t \times 100 \quad (5)$$

Where

d_i : Nominal diameter of the non-corroded rebar in (mm);

i_{corr} : Corrosion current density in ($\mu\text{A}/\text{cm}^2$);

t : Time in years since the initiation of the corrosion.

Figure 2 illustrates the procedure to correct the hysteresis properties of a corroded plastic hinge. A hybrid approach is used in the proposed framework incorporating two methods:

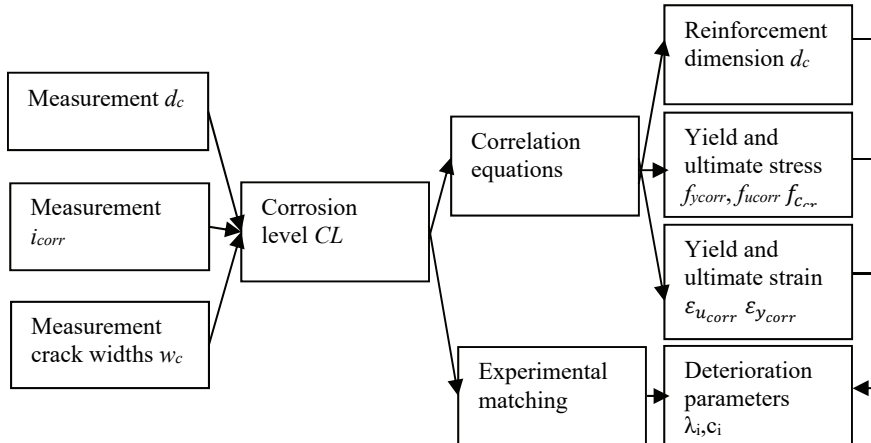


Figure 2 - Corrosion correction of the hysteresis loop parameters

Explicit Method: This method explicitly considers the impact of corrosion on the geometry and material properties of a particular section (hinge) through correlation functions, taking into account the corrosion level (CL).

Implicit Method: The implicit method compensates for the effects of corrosion that cannot be explicitly or directly accounted for in the current study. This includes factors such as stress-strain incompatibility or the loss of bond between reinforcement and concrete. The

implicit method involves either calibrating the degradation parameters or employing a correction factor (interpolation) for the yield moment using a data-based approach.

By combining these explicit and implicit techniques, the proposed framework aims to comprehensively consider the influence of corrosion on the structural behavior, accounting for both known and unidentified corrosion-related effects.

3.2. Corrosion Effect on the Cross Section of the Rebar

Homogeneous corrosion affects the cross-section with more or less uniform loss over the perimeter of reinforcing bars. Localized (or pitting) corrosion, however, concentrates over small areas of the reinforcement. The residual cross-section as reported by several experimental research tests is no longer round with variation in circumference along the bar because of the pitting penetration [31]. Considering Eq. 3, the mean cross-section of the corroded bar (A_c) can be expressed in terms of the degree of corrosion as:

$$A_c = A_i(1 - 0.01CL) \quad (6)$$

All other parameters of the plastic hinge depending on the steel reinforcement sections can be derived from the above relationship.

3.3. Yield and Ultimate Strength and Strain Reduction Due to Corrosion

Numerous studies have been conducted on the stress-strain relationship and the residual strength and ductility capacities of corroded steel reinforcing bars. Within the scope of the present framework, the drop in yield strength and the ultimate strain of the corroded steel reinforcements can be estimated using the formulae proposed by Du et al. [32]:

$$f_{y_{corr}} = f_{y_0}(1 - 0.005CL) \quad (7)$$

$$\varepsilon_{u_{corr}} = \varepsilon_{u_0}(1 - 0.05CL) \quad (8)$$

The altered yield strain, ultimate strength and elastic modulus for uniform corrosion:

$$\varepsilon_{y_{corr}} = \varepsilon_{y_0}(1 - 0.0124CL) \quad (9)$$

$$f_{u_{corr}} = f_{u_0}(1 - 0.0107CL) \quad (10)$$

$$E_{corr} = E_0(1 - 0.0075CL) \quad (11)$$

And for pitting corrosion:

$$\varepsilon_{y_{corr}} = \varepsilon_{y_0}(1 - 0.0198CL) \quad (12)$$

$$f_{u_{corr}} = f_{u_0}(1 - 0.0157CL) \quad (13)$$

$$E_{corr} = E_0(1 - 0.0115CL) \quad (14)$$

3.4. Cracking of Concrete Effect

Cracking of concrete due to corrosion results in a loss of concrete integrity, which reduces the ultimate load capacity of the concrete element [33] and decreases the bond strength [34] which will be accounted for later by the hysteresis degradation parameters calibration. A model proposed by Coronelli and Gambarova, [35] can be used to partially account for the effect of cracked concrete cover on the compression strength. In this model, the reduced compression strength can be determined from:

$$f_{c_{cr}} = \frac{f_c}{1 + 0.1 \frac{\varepsilon_1}{\varepsilon_{c0}}} \quad (15)$$

ε_{c0} is the strain of non-cracked concrete corresponding to compression strength f_c . ε_1 is the average tensile strain of the cracked concrete, which can be calculated as follows:

$$\varepsilon_1 = \frac{n_{bars} w_{cr}}{b_0} \quad (16)$$

Where, b_0 is the width of the element section before cracking, n_{bars} is the number of corroded bars in the cracked concrete width b_0 and w_{cr} is the full width of the crack caused by corroded longitudinal reinforcement and can be calculated as follows:

$$w_{cr} = 2\pi(v_{rs} - 1)P_x \quad (17)$$

$$P_x = 0.0115i_{corr}t \quad (18)$$

P_x , the attack penetration factor, is the average value of corrosion penetration which is the reduction of the bar diameter in (mm), the time t in (years) since the initiation of corrosion and i_{corr} is the corrosion current in ($\mu A/cm^2$). v_{rs} is the volume ratio between the specific volume of a corrosion product and the specific volume of iron, which is taken equal to 2 for steel [36].

By virtue of the above formula and for a given corrosion level CL, the parameters of the MODIMK model are automatically calculated using functions elaborated in Tcl language and implemented into the material library of the OpenSees software.

4. CALIBRATION OF THE DETERIORATING PARAMETERS OF THE HYSTERESIS MODEL

The experimental results of cyclic testing of five columns having different corrosion rates [37] have been used in this study to calibrate the corroded deterioration factors of MODIMK hysteresis model. For this purpose, the specimens are modeled using an elastic element connected to a zero-length element that serves as a plastic hinge to represent the nonlinear behavior of the element. Translational DOFs are constrained to one end of the elastic element through the "equal DOF" command. The specimen geometry and the corresponding numerical model are shown in Fig. 3.

4.1. Description of the Experimental Specimens

Five RC specimens with corrosion percentages of 0%, 5.1%, 8.3%, 13.25% and 16.8% of the reinforcing steel at their bases have been tested [37]. The electrochemical method was employed to artificially induce corrosion in the rebar and stirrups. The extent of corrosion was evaluated theoretically using Faraday's method, while the average mass losses in various regions of the specimens were determined experimentally by weighing the amount of corrosion after testing, as described in reference [37]. The cross-sections and heights of the five specimens are identical with similar longitudinal reinforcing bars and transverse stirrups. The specimen dimensions together with the reinforcement details are given in Fig. 3. The compressive strength f_c is 46.4 MPa. More details on reinforcements and material properties of the steel and concrete are given in the reference [37]. A constant axial load ratio of 0.18 and increasing cyclic lateral displacement control loading protocol [37] were applied on each specimen.

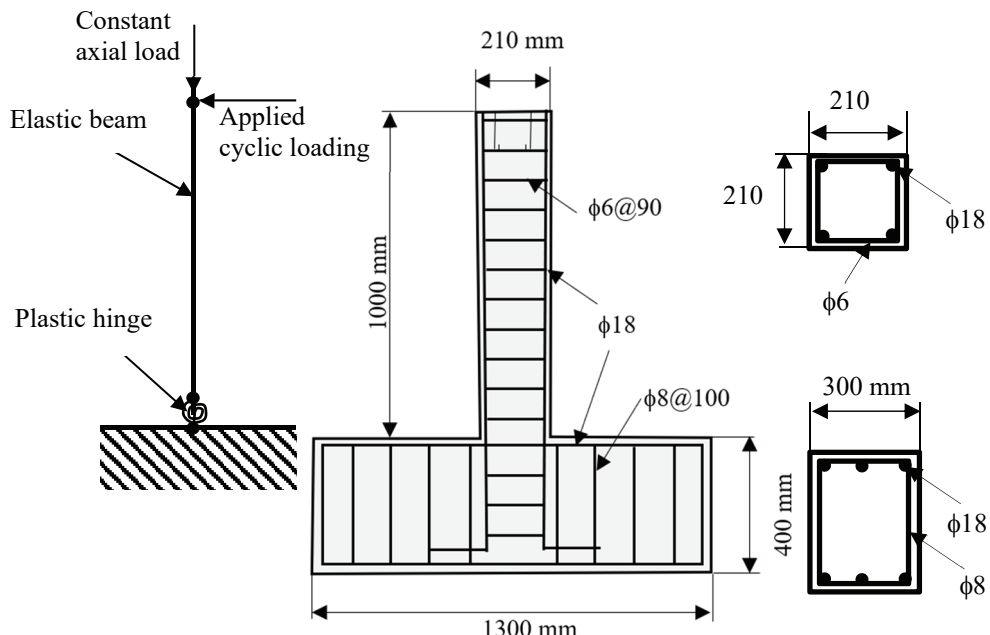


Figure 3 - Test specimen dimensions and the numerical model [37]

The changing values of the model parameters: My^+ , My^- , Ke , θ_{pc} , for the five specimens and for different corrosion level (CL) are shown in Table 1. The values of the following parameters remain unchanged: $\theta_p^+ = 0.019$ rad, $\theta_p^- = 0.019$ rad and $Mc/My = 1.17$

Table 1 - Modified hysteresis parameters

CL(%)	My ⁺ (KN.m)	My(KN.m)	Ke(KN.m)	$\theta_{pc}^+(rad)$ $\theta_{pc}^-(rad)$
0	58.68	58.68	14466.6	0.054
5.1	58.33	58.33	14478.4	0.054
8.3	58.13	58.13	14485.8	0.054
13.25	57.60	57.60	14505.7	0.053
16.8	51.54	51.54	14505.7	0.053

4.2. Calibration Procedure of the Cyclic Degradation Parameters for Different Corrosion Levels

As mentioned before, the effect of the reinforcement corrosion on the geometrical and mechanical characteristics of the RC elements have been explicitly considered using correlation functions. However, there are additional effects of the corrosion level that have not been explicitly accounted for. These effects will be compensated for through a calibration procedure to match the rate of degradation under cyclic loading. The MODIMK hysteresis model provides four degradation parameters $\lambda_A, \lambda_K, \lambda_S, \lambda_C$ and their exponents C_A, C_K, C_S, C_C to control the deterioration of the loading strength, post capping strength, the loading, and unloading stiffness, respectively. A calibration procedure based on random-mutation hill-climbing (RMHC) algorithm is used to fine-tune the values of these parameters for different levels of corrosion. This optimization technique is believed to be suitable for this case because local optimum values are sought [38]. The starting values of the parameters p_i ($i=1$ to 8) corresponding to $\lambda_A, \lambda_K, \lambda_S, \lambda_C, C_A, C_K, C_S, C_C$ respectively are chosen within the intervals of variation and then iteratively the algorithm progresses to find a better solution by making an incremental change starting from the initial solution.

The degradation parameters λ_i have an appreciable effect for values equal to 10 or smaller. A zero value is assigned to deactivate the degradation effect. The variation range of the exponential factors C_i vary from 1.0 for constant rate of deterioration to 2.0 for slow down rate of deterioration at initial cycles and increased rate of deterioration in subsequent cycles [21,39].

Therefore, in the hill-climbing algorithm, the ranges of variation of the degradation parameters are taken in the intervals [0. 10.] for λ_i ($p_{i=1 \text{ to } 4}$) and [1.0 2.0] for C_i ($p_{i=5 \text{ to } 8}$). Both ranges have been normalized with respect to their relative maximal and minimal values (boundaries of the intervals) and subdivided into $N_p=100$ increments each.

The algorithm keeps improving the solution by making incremental changes $\Delta p_{i,k}$ until it converges to an optimal solution or it stops for a given limit of iterations. The objective function aims to follow as closely as possible the experimental (reference) force-displacement hysteresis loops. In addition to the strength and stiffness cyclic variations, it reflects the energy dissipated by the RC specimen at the plastic hinge. For N digitalized experimental and numerical pairs $(F_{exp,i}, \theta_i)$, $(F_{mod,i}, \theta_i)$ respectively, corresponding to a corrosion level (test), the algorithm minimizes the relative error given for each iteration k by:

$$e_k = \sqrt{\sum_{i=1}^N \left(\frac{F_{mod,i} - F_{exp,i}}{F_{exp,i}} \right)^2} \quad (19)$$

With an acceptance criterion:

$$\frac{e_{k+1} - e_k}{e_k} < e_l \quad (20)$$

An error $e_k = 1\%$ is considered precise enough to terminate the optimization process or a limit of 200 iterations. It should be noted also that the acceptance criterion e_l for an adjustment has been given a positive value to avoid a premature convergence of the objective function towards local minima [38].

The cyclic degradation parameters and their exponents (λ_i and c_i) for specimen with increasing levels of corrosion obtained from the calibration with the experimental tests are given in Table 2. It should be noted that the effect of individual deterioration parameters can compensate each other's, therefore the calibration process is not firmly robust.

Table 2 - Calibrated cyclic degradation parameters

CL (%)	λ_c	λ_A	λ_K	λ_s	c_c	c_A	c_K	c_s
0	1	1	1	1	1	1	1	1
5.1	6.8	0.3	0.3	0.4	1.02	1.06	1.01	1.01
8.3	7.3	0.4	0.1	0.6	1.13	1.04	1.20	1.24
13.25	7.1	0.4	0.2	0.7	1.12	1.31	1.40	1.51
16.8	7.0	0.5	0.1	0.7	1.10	1.16	1.21	1.46

Representative hysteresis loops of the specimens before reaching the ultimate state are given in Fig. 4. The maximum number of loading cycles varies from 14 cycles for specimens ZZ-1 to 12 cycles for specimen ZZ-5. The number of loading cycles decreases with increasing degrees of corrosion.

Default values of the degradation parameters for 0% corrosion where all degradation parameters are set to unity as given in Table 2, were used for specimen ZZ-1 which resulted in large discrepancies between the numerical and experimental curves. Calibration of the degradation parameters were made for corroded specimens and gave an acceptable approximation except for ZZ-5 sample where the last maximum lateral load dropped sharply compared to the previous ones ZZ-3 and ZZ-4. This can be attributed to buckling of longitudinal reinforcement because of the transverse reinforcement corrosion that has not been accounted for explicitly. Therefore, for specimen ZZ-5 with 16.8% corrosion, the yield moment has been adjusted using a correction coefficient of the moment $\alpha = 0.85$. If additional data becomes available, it is possible to further calibrate the value of the correction factor α specifically for higher levels of corrosion.

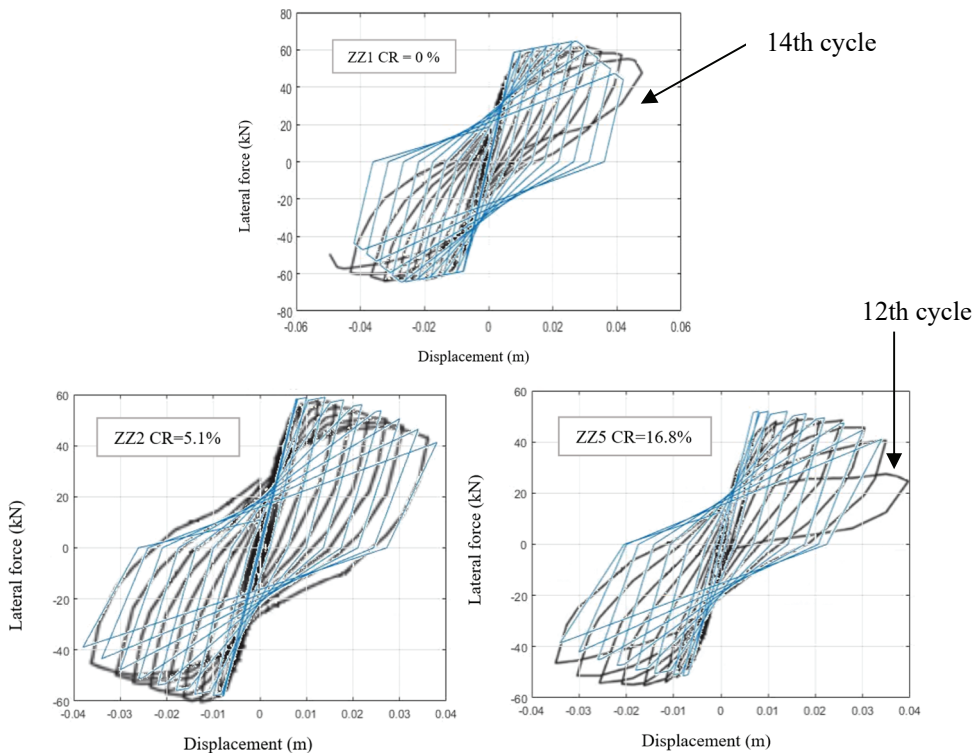


Figure 4 - Experimental and numerical hysteresis loops for samples with corrosion levels: 0% for ZZ-1, 5.1% for ZZ-2 and 16.8% for ZZ-5 [37]

5. NONLINEAR DYNAMIC PERFORMANCE OF A BRIDGE WITH CORRODED PIERS

This section is dedicated to the evaluation of the effect of the corrosion of the steel reinforcement on the seismic response of a typical full scale bridge structure.

5.1. Description of the Bridge Structure

The choice of the structure was dictated by the availability of data for the calculation of the parameters governing the constitutive law and the availability of some results of previous work [40] for comparison and validation of the model. The chosen structure is a regular straight bridge consisting of a deck resting on six prefabricated NEBT 1600 (New England Bulb Tee) prestressed girders supported by a three-column pier system. The deck consists of two continuous spans of 36 m long and 13 m wide (Fig. 5).

The columns are constituted of rectangular cross-section of 1.2 m deep and 0.6 m wide. The design was carried out according to the requirements of the Canadian Bridge Code CSA-S6

[41]. The columns extend into the foundation and the pier cap for a distance of 0.5 m. The height of the columns and the pier cap are 6 m and 1m, respectively, bringing the total height of the frame to 7 m.

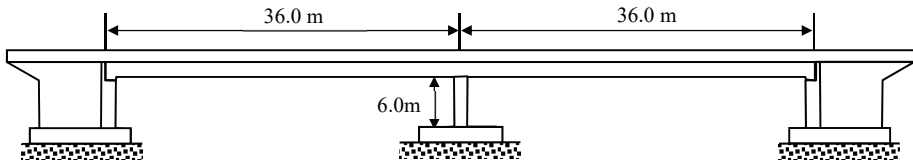


Figure 5 - Longitudinal elevation and dimensions of the studied bridge

5.2. OpenSees Model

The deck is segmented into two linear elastic column-beam elements. The piers are also modeled as column-beam elements adopting linear elastic behavior with zero-length springs (plastic hinges) added at the ends idealizing the nonlinear behavior in the plastic hinges. The pier cap was taken very rigid to allow the plastic hinge to develop properly at the foot and head of the piers.

The geometry of the model is composed of 7 elastic beam elements and 6 nonlinear zero-length hinges using uniaxial Ibarra-Medina-Krawinkler "peak oriented" material. The degrees of freedom of translation and rotation in two directions of the hinges are linked to the element nodes via the "equal DOF" command (Fig. 6).

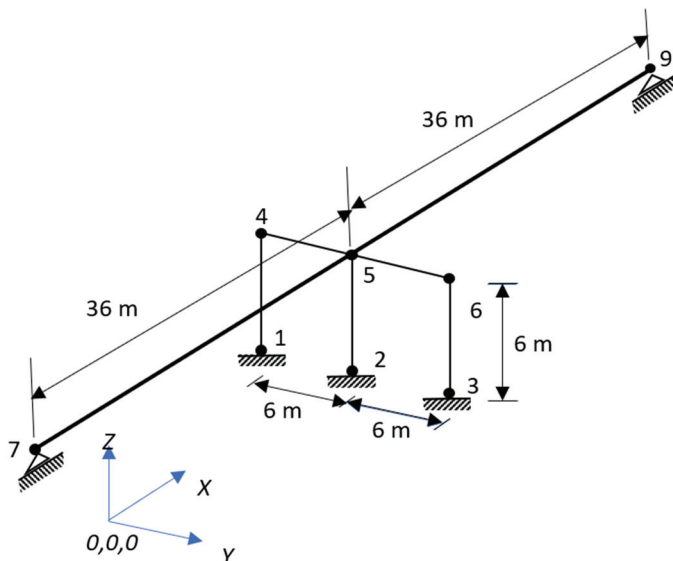


Figure 6 - OpenSees model of a typical bridge with plastic hinges (MODIMK)

It is assumed that the corrosion degradation is uniform, meaning that the level of corrosion is identical for all hinges during the same analysis and it varies from 0% (undamaged structure) to a corrosion rate of 20%.

The hysteresis parameters depending on the geometric and material properties of the steel reinforcement and concrete are computed for sound and corroded sections for corrosion rates of 0% and 20% using the correction factors of Eqs.5-18. The degradation parameters of MODIMK model have been calibrated for a corrosion degree varying from 0% to 16.80%. Due to a lack of experimental data above this level, the performance analysis is limited to 20% of corrosion rate. The cyclic degradation parameters in the MODIMK model and their exponents have been extrapolated by curve fitting the results of the calibration phase up to 20% (Table 3).

Table 3 - Cyclic degradation parameters and their exponents

CL (%)	λ_C	λ_A	λ_K	λ_S	C_C	C_A	C_K	C_S
20	7.12	0.65	0.42	0.95	1.10	1.11	1.27	1.29

The yield moment M_y is corrected using the same value $\alpha = 0.85$.

5.3. Seismic Loading and Nonlinear Dynamic Analysis

A dataset composed of four records of horizontal components of real earthquakes, and two artificial accelerograms are selected to best cover the RPA99 seismic code spectrum [42] and applied as a representative seismic loading of a high seismic zone. The artificial accelerograms are generated using ‘seismoArtif’ software [43]. The main characteristics of the selected acceleration time histories are given in Table 4. and Fig. 7 shows the mean response spectra of the six accelerograms closely covering the target site spectrum.

Table 4 - Characteristics of the accelerograms

Accelerograms	PGA(g)	Field	Duration (s)
Manjil	0.515	Far	52.0
Northridge	0.568	Near	38.0
Dar El Beida	0.341	Far	55.3
Friuli	0.531	Near	36.3
Artif 1	0.618	Far	20.0
Artif 2	0.599	Near	11

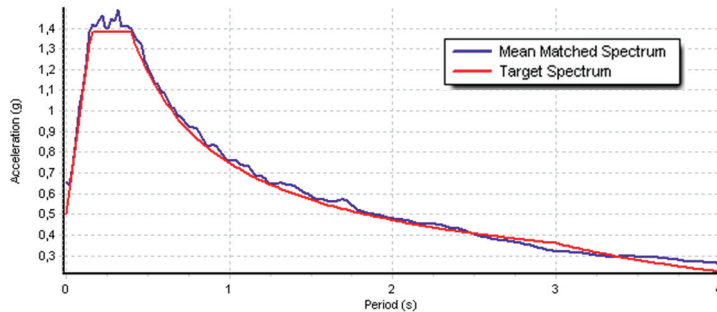


Figure 7 - The target seismic code spectrum and the mean spectrum of the different accelerograms

The performance of the structure is evaluated in terms of the structural responses of the hysteresis loops, the maximum lateral displacements and the dissipated energy.

5.4. Effect of the Corrosion Level on the Displacement Response Under Different Earthquake Ground Motions

Representative displacement time histories of the bridge deck along the longitudinal direction under the far-field Artif1 earthquake and the near-field Friuli earthquake are shown in Figs. 8 and 9. The effect of the corrosion is more pronounced under Artif1 accelerogram and the

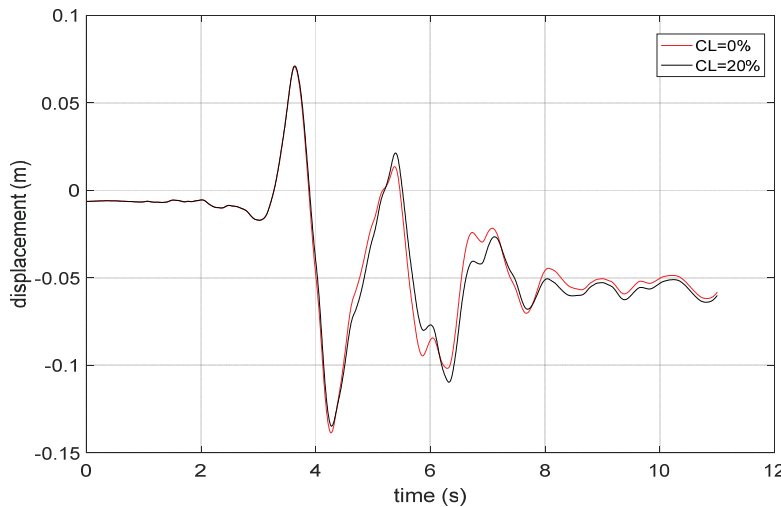


Figure 8 - Lateral displacement responses under Friuli

peak displacement increases with increasing CL. Permanent deformation, which is an important indicator of damage, is observed at the end of the action effects. This residual displacement is highly dependent on the loading conditions. For a 20% corrosion level, it reaches 1.64 times the displacement of the uncorroded model under the far-field Artifl earthquake. However, it remains almost the same under the near-field Friuli earthquake.

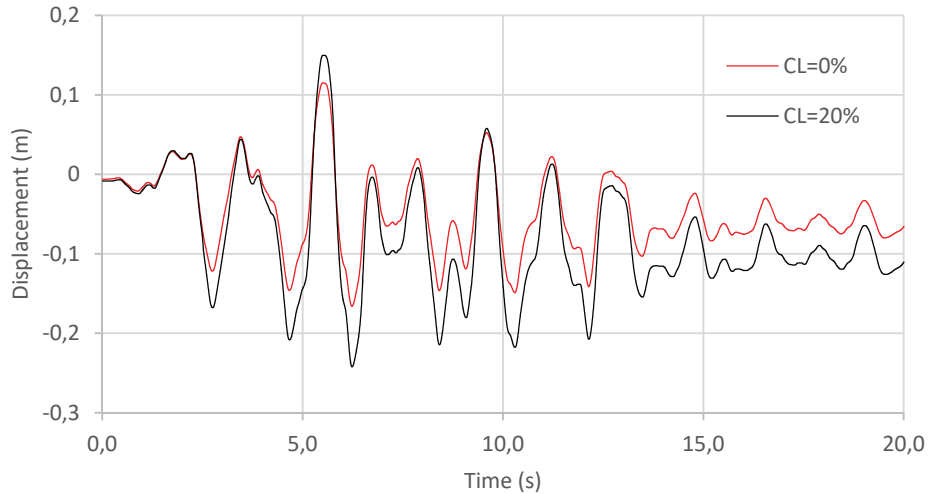


Figure 9 - Lateral displacement responses under Artifl

The hysteresis loops of the different plastic hinges are more regular for far-field accelerograms compared to near-field accelerograms as represented by the results of the Friuli and Artifl accelerograms in Fig. 10. Deteriorations of strength, stiffness and pinching are more noticeable in corroded hinges.

The corrosion effect is more pronounced for severe ground acceleration. Table 5 shows the percentage increase in displacements and plastic rotations for increasing ground acceleration intensity (Artifl) scales.

Where:

$$\Delta D_{max} = \frac{(D_{CL} - D_{CL0})}{(D_{CL0})} \times 100\% \quad (21)$$

$$\Delta \theta_{max} = \frac{(\theta_{CL} - \theta_{CL0})}{(\theta_{CL0})} \times 100\% \quad (22)$$

With:

D_{CL} et θ_{CL} displacement and plastic rotation corresponding to corrosion rate CL;

D_{CL0} et θ_{CL0} displacement and plastic rotation corresponding to CL=0.

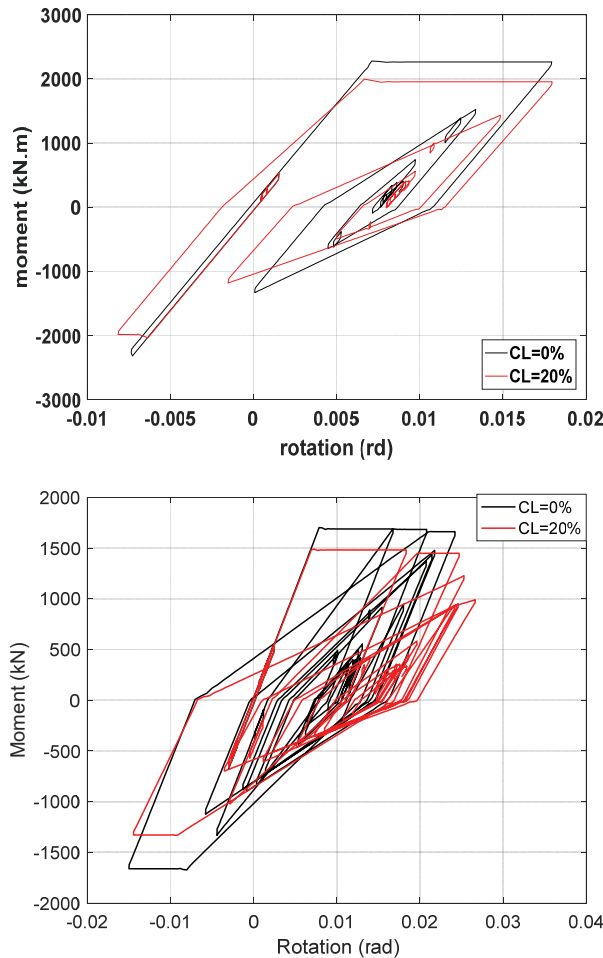


Figure 10 - Hysteresis loop responses under Friuli and Artifl accelerograms

Table 5 - Displacements and plastic rotations for increasing loading intensity at different corrosion levels

	Scale = 1.0		Scale = 1.5		Scale = 2.0	
CL	ΔD_{max}	$\Delta \theta_{max}$	ΔD_{max}	$\Delta \theta_{max}$	ΔD_{max}	$\Delta \theta_{max}$
20%	0	3.76	2.25	11.9	15.08	23.63

5.5. Effect of the Corrosion Level on the Hysteresis Energy Dissipation Capacity

Figure 11 shows the dissipated energy curve under Artifl accelerogram for 0% and 20% corrosion level. It can be noticed that the dissipation energy decreases with increasing CL

which has been also reported in the literature [44]. This trend is not perceived under Friuli accelerogram (Fig. 12), where the energies for the different corrosion levels are comparable. The energy dissipated at CL = 20% is slightly higher than CL=0%. This can be attributed to the fact that the strength and stiffness degradations are compensated by an early yielding and larger plastic rotations.

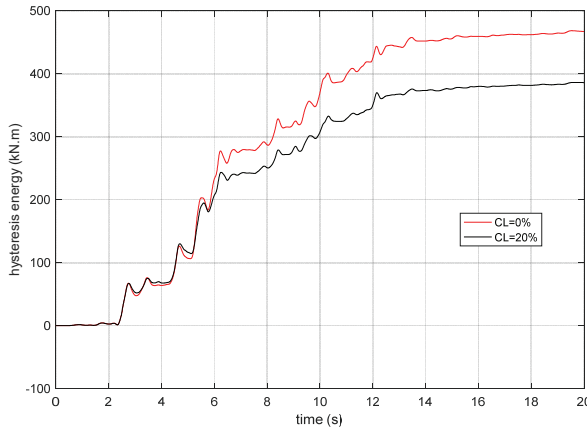


Figure 11 - Energy dissipated under Artificial earthquake

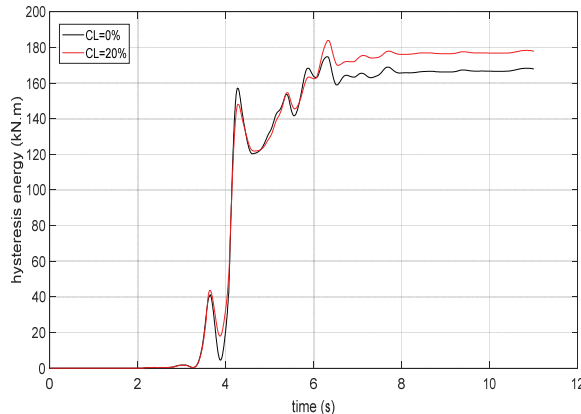


Figure 12 - Energy dissipated under Friuli earthquake

6. CONCLUSION

A major durability concern for RC infrastructures in aggressive environment is steel reinforcement corrosion. The trend of seismic codes towards new predictive generations suggests explicit quantifications of degradation parameters to be integrated into nonlinear dynamic analyses in the design phase or for structural assessment of existing buildings.

A framework for the application of a corrosion dependent geometric and material properties together with degradation hysteresis parameters of a RC element section has been put in place. For this purpose, a corrosion level indicator that can be obtained from in-situ measurements or predicted by a time-dependent approach is used to adjust the geometric and material properties of a corroded RC section. The adjustment functions are implemented into the material library of the OpenSees software to automatically calculate the parameters of the MODIMK model. The cyclic degradation parameters and their exponents (λ_i and c_i) are fine-tuned using a random-mutation Hill-Climbing (RMHC) algorithm for a range of corrosion levels corresponding to available experimental data. It should be noted that the yield moment, in addition to the geometric and material properties alteration, needs to be reduced by an extrapolated factor α to account for transverse reinforcement corrosion and other effects that have not been compensated for explicitly.

To investigate the effect of the corrosion on the seismic behavior of structures, a typical full scale two spans bridge model having three piers with increasing uniform corrosion levels has been studied under several earthquake ground accelerations. The performance of the bridge has been evaluated using lateral displacements, plastic rotations and hysteresis energy dissipation audit. The results showed that the effect of corrosion highly dependent on the intensity and type of earthquake ground motions. Within the limit of the considered seismic loading, the permanent displacement (taken as an indicator of damage) reached 1.64 times for a corrosion level of 20%. The general trend is that the corroded piers are less dissipative, however in some cases where the dissipated hysteresis energy was comparable for the corroded and saline structure, the plastic hinges at the ends of the corroded piers undergo excessive plastic rotations.

Although, the proposed protocol can be used for practical issues where seismic performance prediction or structural assessment are sought for design or existing structures, further work and research are required to complete and improve the robustness of the calibration process for full scale specimen with higher corrosion levels.

Acknowledgements

The financial support of the Ministry of higher education MESRS in Algeria (Grant CNEPRU J0400420140001) for conducting this study is greatly acknowledged.

References

- [1] Li W., Xu C., Ho S.C., Wang B., Song G., Monitoring concrete deterioration due to reinforcement corrosion by integrating acoustic emission and FBG strain measurements. *Sensors*. 2017;17(3):657. <https://doi.org/10.3390/s17030657>
- [2] Bertolini L., Elsener B., Pedeferrri P., Redaelli E., Polder R., Corrosion of steel in concrete: Prevention, diagnosis, repair (2nd ed.); Weinheim, Germany: Wiley VCH; 2013.
- [3] Andrade C., Propagation of reinforcement corrosion: principles, testing and modelling, *Mater Struct*. 2019; 52:2, <https://doi.org/10.1617/s11527-018-1301-1>

- [4] François R., Laurens S., Deby F., Steel corrosion in reinforced concrete, Editor(s): Raoul François, Stéphane Laurens, Fabrice Deby, Corrosion and its consequences for reinforced concrete structures, Elsevier, 2018; 1-41, ISBN 9781785482342, <https://doi.org/10.1016/B978-1-78548-234-2.50001-9>
- [5] Bertolini L., Steel corrosion and service life of reinforced concrete structures, *Struct Infrastruct Eng.* 4:2, 123-137, <http://dx.doi.org/10.1080/15732470601155490>
- [6] Şengül, Ö. (2011). Probabilistic Design for the Durability of Reinforced Concrete Structural Elements Exposed to Chloride Containing Environments . *Teknik Dergi* , 22 (110) , 1461-1475, <https://dergipark.org.tr/en/pub/tekderg/issue/12749/155174>
- [7] Andisheh K., Scott A., Palermo A., Seismic behavior of corroded RC bridges: Review and research gaps, *Int J Corros.* 2016, Article ID 3075184, <http://dx.doi.org/10.1155/2016/3075184>.
- [8] Inci P., Goksu C., Ilki A., Kumbasar N., Effects of reinforcement corrosion on the performance of RC frame buildings subjected to seismic actions. *Journal of Performance of Constructed Facilities*, 27(6), 683–696. doi:10.1061/(ASCE)cf.1943-5509.0000378
- [9] Nataraj S., Hogan L., Scott A., Ingham J., Simplified Mechanics-Based Approach for the Seismic Assessment of Corroded Reinforced Concrete Structures *J Struct Eng.*, 2022, 148(3), 04021296, doi:10.1061/(ASCE)ST.1943-541X.0003265.
- [10] Opabola E. A., Residual seismic capacity of beam-column components with corroded reinforcement, *Constr. Build. Mat.* 332 (2022) 127269, <https://doi.org/10.1016/j.conbuildmat.2022.127269>
- [11] Bourahla N., Tafraout S., Attar A., Nonlinear dynamic response of aging degraded reinforced concrete structures under earthquake loading, Proceedings of the 14th European Conference on Earthquake Engineering, Ohrid Macedonia 2010, paper 537.
- [12] Akiyama M., Frangopol D.M., Long-term seismic performance of RC structures in an aggressive environment: emphasis on bridge piers, *Struct Infrastruct Eng.* 2014;10:7, 865-879, doi: 10.1080/15732479.2012.7612
- [13] Choe D.E., Gardoni P., Rosowsky D., Haukaas T., Seismic fragility estimates for reinforced concrete bridges subject to corrosion. *Struct. Saf.*, 2009;31(4), 275-283. doi:10.1016/j.strusafe.2008.10.001
- [14] Hu S., Wang Z., Guo Y., Xiao G., Life-cycle seismic fragility assessment of existing RC bridges subject to chloride-induced corrosion in marine environment. *Adv Civ Eng.* 2021, Article ID 9640521, 18 pages, <https://doi.org/10.1155/2021/964052>
- [15] Domaneschi M., De Gaetano A., Casas J.R., Cimellaro G.P., Deteriorated seismic capacity assessment of reinforced concrete bridge piers in corrosive environment. *Struct Concr.* 2020;1–16. <https://doi.org/10.1002/suco.202000106>
- [16] Naderpour H., Ghasemi-Meydansar F., Haji M., Experimental study on the behavior of RC beams with artificially corroded bars, *Structures*, Volume 43, 2022, pp1932-1944, <https://doi.org/10.1016/j.istruc.2022.07.005>.

- [17] Goksu C. and Ilki A., Seismic behavior of reinforced concrete columns with corroded deformed reinforcing Bars, *ACI Structural Journal* 113 (5) 2016: 1053-1064, DOI:10.14359/51689030
- [18] Meda A., Mostosi S., Rinaldi Z., Riva P., Experimental evaluation of the corrosion influence on the cyclic behaviour of RC columns. *Eng Struct.* 2014; 76: 112 – 123. doi:10.1016/j.engstruct.2014.06.043
- [19] Kim T.H., Seismic performance assessment of deteriorated two-span reinforced concrete bridges. *Int J Concr Struct Mater* 2022; 16:4 <https://doi.org/10.1186/s40069-022-00498->
- [20] Scattarreggia N., Qiao T., Malomo D., Earthquake response modeling of corroded reinforced concrete hollow-section piers via simplified fiber-based FE analysis. *Sustain* 2021; 13, 9342. <https://doi.org/10.3390/su13169342>
- [21] Ibarra L.F., Medina R.A., Krawinkler H., Hysteretic models that incorporate strength and stiffness deterioration, *Earthq Eng Struct Dyn*, 2005; 34(12), 1489-1511. <https://doi.org/10.1002/eqe.495>
- [22] McKenna F., OpenSees: A Framework for earthquake engineering simulation, *Comput Sci Eng.* 2011; 13(4), 58-66, doi:10.1109/MCSE.2011.66.
- [23] Haselton C.B., Liel A.B., Lange S.T., Deierlein G.G., Beam-column element model calibrated for predicting flexural response leading to global collapse of RC frame buildings, PEER Report 2007/03, PEER Center, University of California, Berkeley, 2008.
- [24] Panagiotakos T.B., Fardis M.N., Deformations of reinforced concrete at yielding and ultimate, *ACI Struct J*, 2001; 98(2), 135-147.
- [25] Özyurt N., Söylev T. A., Özturan T., Pehlivan A.O., Niş A., Corrosion and chloride diffusivity of reinforced concrete cracked under sustained flexure. *Teknik Dergi* 31 2020: 10315-10337
- [26] Bezuidenhout S.R., Van Zijl G.P.A.G., Corrosion propagation in cracked reinforced concrete, toward determining residual service life. *Struct Concr.* 2019;1–11. <https://doi.org/10.1002/suco.201800275>
- [27] Bossio A., Lignola G.P., Fabbrocino F., Monetta T., Prota A., Bellucci F., Manfredi G., Nondestructive assessment of corrosion of reinforcing bars through surface concrete cracks, *struct concr.* 2017;18(1), 104-117. <https://doi.org/10.1002/suco.201600034>.
- [28] Khan I., François R., Castel A., Prediction of reinforcement corrosion using corrosion induced cracks width in corroded reinforced concrete beams. *Cem. Concr. Res.* 2014, 56, 84–96. <https://doi.org/10.1016/j.cemconres.2013.11.006>
- [29] Nikoo M., Sadowski Ł., Nikoo M., Prediction of the corrosion current density in reinforced concrete using a self-organizing feature map. *Coatings* 2017; 7, 160. <https://doi.org/10.3390/coatings7100160>
- [30] Du Y.G., Clark L.A., Chan A.H.C., Effect of corrosion on ductility of reinforcing bars. *Mag Concr Res.* 2005; 57(7), 407-419. doi:10.1680/macr.2005.57.7.407

- [31] González J.A., Andrade C., Alonso C., Feliu S., Comparison of rates of general corrosion and maximum pitting penetration on concrete embedded steel reinforcement. *Cem. Concr. Res.* 1995; 25(2), 257–264. doi:10.1016/0008-8846(95)00006-2
- [32] Du Y.G., Clark L.A., Chan A.H.C., Residual capacity of corroded reinforcing bars, 2005, *Mag Concr Res.* 57(3), 135-147. doi:10.1680/macr.2005.57.3.135
- [33] Tapan M., Aboutaha R.S., Effect of steel corrosion and loss of concrete cover on strength of deteriorated RC columns, *Constr. Build. Mat.* 25 (2011) 2596–2603, doi:10.1016/j.conbuildmat.2010.12.003
- [34] Apostolopoulos C., Koulouris K.F., Apostolopoulos A.C., Correlation of surface cracks of concrete due to corrosion and bond strength (between steel bar and concrete), *Advances in Civil Engineering*, vol. 2019, Article ID 3438743. <https://doi.org/10.1155/2019/3438743>
- [35] Coronelli D., Gambarova P., Structural assessment of corroded reinforced concrete beams: Modeling guidelines. *J Struct Eng.* 2004;130(8), 1214–1224. doi:10.1061/(asce)0733-9445(2004)130:8(1214).
- [36] Poursaei A., Corrosion of steel in concrete structures, 1st Edition, Woodhead Publishing, ISBN - 13:9781782423812.
- [37] Yang S.Y., Song X.B., Jia H.X., Chen X., Liu X.L., Experimental research on hysteretic behaviors of corroded reinforced concrete columns with different maximum amounts of corrosion of rebar. *Construct Build Mater.* 2016; 121, 319–327. doi:10.1016/j.conbuildmat.2016.06.002
- [38] Taborda D.M.G., Zdravkovic L., Application of a Hill-Climbing technique to the formulation of a new cyclic nonlinear elastic constitutive model. *Comput Geotech.* 2012; 43, 80–91. doi:10.1016/j.comgeo.2012.02.001
- [39] Ibarra L., Krawinkler H., Global collapse of frame structures under seismic excitations. Blume Center TR 152, Stanford University; 2003.
- [40] Khaled A., Tremblay R., Massicotte B., Combination rule for the prediction of the seismic demand on columns of regular bridges under bidirectional earthquake components. *Can J Civ Eng.* 2011 38(6), 698–709. doi:10.1139/l11-031
- [41] Canadian Standard Association (CSA). CSA-S6: Canadian Highway Bridge Design Code. Rexdale, ON, 2006.
- [42] RPA99 version 2003, Algerian Seismic Regulations, DTR BC 2.48, Earthquake Engineering National Research Centre, Algiers, 9961-923-13-8, 2004.
- [43] Seismosoft 2020, SeismoArtif – A computer program for generation of artificial accelerograms. Available from URL: www.seismosoft.com accessed 12-03-2021.
- [44] Celik A., Yalciner H., Kumbasaroglu A., Turan A.I., An experimental study on seismic performance levels of highly corroded reinforced concrete columns. *Struct Concr.* 2021;1–19. <https://doi.org/10.1002/suco.202100065>

